Broadband, Ultrafast, Self-Driven Photodetector Based on Cs-Doped $FAPbI_3$ Perovskite Thin Film

*Feng-Xia Liang, Jiu-Zhen Wang, Zhi-Xiang Zhang, You-Yi Wang, Yang Gao, and Lin-Bao Luo**

In this study, a high-performance photodetector comprised of formamidinium cesium lead iodide ($FA_{1-x}Cs_xPbI_3$) thin film is developed. The Cs-doped $FAPbI_3$ perovskite material is synthesized through a simple spin-coating method, via which $FA_{1-x}Cs_xPbI_3$ with different Cs doping levels (x = 0.1, 0.15, 0.2, and 0.3) can be obtained. Further optoelectronic characterization reveals that the $FA_{0.85}Cs_{0.15}PbI_3$ photodetector exhibits reproducible sensitivity to irradiation with wavelengths in the range from 240 to 750 nm, whereas it is weakly sensitive to wavelengths longer than 750 nm. The responsivity and specific detectivity are estimated to be around 5.7 A W^{-1} and 2.7×10^{13} cm $Hz^{1/2}$ W^{-1}, respectively. It is also worth noting that the present perovskite photodetector demonstrates an ultrafast response speed (t_r/t_f: 45 ns/91 ns) at zero bias voltage, which is probably related to the ultrafast lifetime and high quality of thin film according to the Hall effect study. Finally, this device shows a weak degradation in sensitivity to white light after storage at ambient condition for 45 days. The totality of the broadband sensitivity, high specific detectivity, ultrafast response speed, and self-driven property renders the $FA_{1-x}Cs_xPbI_3$ an idea material for high-performance photodetectors application.

1. Introduction

Photodetector, as a typical example of optoelectronic devices, is able to detect light illumination with wavelength ranging from ultraviolet to infrared. It has attracted increasing research interest recently owing to its promising application in safety monitoring, spatial optical communication, chemical/biological imaging, and light vision.[1–3] Hitherto, tremendous efforts have been devoted to the design of wide broadband light harvesting structures through the combination of different functional materials.[4–6] However, the fabrication methods are usually complicated or employing expensive instruments. The recent discovery of a group of organolead halide perovskites ($APbX_3$) has provided promising routes to high-performance optoelectronic devices application.[7–9] Various study has demonstrated that perovskite materials can display many unique properties such as direct bandgap, large absorption coefficient, long charge diffusion length, low density of defects, and easy fabrication, which makes them extremely attractive in photodetector applications.[10–13] For instance, Lee et al. developed a novel hybrid photodetector comprised of graphene and $CH_3NH_3PbI_3$ thin film. The photodetector had a broadband photoresponsivity from 400 to 800 nm, with a response time of 87 (rise time) and 540 ms (fall time). What is more, the photoresponsivity and effective quantum efficiency were 180 A W^{-1} and 5×10^4% at a relatively high illumination power of 1 μW, respectively.[14] Very recently, Jie's group reported the fabrication of a high-performance photodetector based on single-crystalline aligned $CH_3NH_3PbI_3$ microwire arrays, which were synthesized by a facile blade-coating approach. It was observed that the device displayed apparent sensitivity to visible light illumination with very good reproducibility. According to their calculation, the device exhibited a high responsivity of 13.5 A W^{-1} at visible light, with a response time of 80 (rise time) and 240 μs (fall time).[15] In spite of the above achievements, it is inevitable to point out that the above devices are characterized by relatively low specific detectivity and slow response speed, which greatly limit their further applications. In addition, most of the perovskite photodetectors need external bias voltage.[16–18] Here, in this study, we report a high-performance photodetector based on formamidinium cesium lead iodide ($FA_{1-x}Cs_xPbI_3$), which has a band gap of 1.51 eV and has demonstrated to be ideal material for photovoltaic devices application.[19] The $FA_{1-x}Cs_xPbI_3$ film was synthesized through a one-step spin-coating strategy. SEM study revealed that when x is equal to 0.15, continuous perovskite thin film with high quality can be obtained. It is also revealed that the $FA_{0.85}Cs_{0.15}PbI_3$ shows obvious sensitivity to light illumination with wavelengths ranging from UV to Vis light (240–750 nm). The responsivity and specific detectivity were estimated to be 5.7 A W^{-1} and 2.7×10^{13} cm $Hz^{1/2}$ W^{-1}, which are much better than most of other $MAPbI_3$ thin film

Dr. F.-X. Liang, J.-Z. Wang
School of Materials Science and Engineering
Hefei University of Technology
Hefei 230009, China

Z.-X. Zhang, Y.-Y. Wang, Y. Gao, Prof. L.-B. Luo
School of Electronic Science and Applied Physics
Hefei University of Technology
Hefei 230009, China
E-mail: luolb@hfut.edu.cn

The ORCID identification number(s) for the author(s) of this article can be found under https://doi.org/10.1002/adom.201700654.

DOI: 10.1002/adom.201700654

and single crystal-based devices. Besides, our photodetector could operate without bias voltage, demonstrating good self-powered properties. It is believed that the present broadband, ultrafast, and self-driven perovskite film-based photodetector will have potential application in future optoelectronic devices and systems.

2. Results and Discussion

The cesium-doped $FaPbI_3$ film ($FA_{1-x}Cs_xPbI_3$) was synthesized by a simple spin-coating strategy, as illustrated by the scheme in **Figure 1**a. Briefly, a mixed solution containing PbI_2, $HC(NH_2)_2I$ (FAI), and CsI was first spin-coated onto a glass film. After rinsing with diethyl ether solution, the sample was thermally treated at 50 °C for 3 min, followed by 140 °C for 15 min. According to the digital camera picture and structural diagram shown in Figure 1a, the as-synthesized $FA_{1-x}CS_xPbI_3$ perovskite film is black-brownish in color. What is more, like the traditional $MAPbX_3$, the present $FA_{1-x}Cs_xPbI_3$ has a similar structure: the FA^+ and Cs^+ cations occupy the eight corner of the cubic unit cell, while the Pb atom resides at the center of the body of a $[PbI_6]^{4-}$. In order to reveal the influence of FA concentration on the perovskite structure, X-ray diffraction (XRD) patterns of four $FA_{1-x}Cs_xPbI_3$ samples with different Cs ratios ($x = 0.1$, 0.15, 0.2, and 0.3) are studied. As shown in Figure 1b, for the $FA_{1-x}Cs_xPbI_3$ films with Cs doping level from 0.10 to 0.15 and 0.20, the corresponding diffraction peaks could be all indexed to the black phase of $FAPbI_3$.[20] However, when the x further increases to 0.3, new phase due to $CsPbI_3$ begins to appear. Figure 1c–e shows the corresponding field emission scanning electron microscopy (FESEM) images of the perovskite film. It is apparent to find that when x is equal to 0.1 or 0.2, discontinuous film with obvious holes or defects will be formed. This result is in sharp contrast to the case of $x = 0.15$, where relatively high quality perovskite with continuous film was obtained. From the atomic force microscopy (AFM) topography image shown in Figure 1f, the average roughness of $FA_{0.85}Cs_{0.15}PbI_3$ is estimated to be around 150 nm. Further normalized photoluminescence spectra in Figure 1g reveal that with the increase of x from 0.1 to 0.15 and 0.2, the peak of the $FA_{1-x}Cs_xPbI_3$ film will blue shift from 789.1 to 784.7 and 779.5 nm, which is slightly different from previous study.[21]

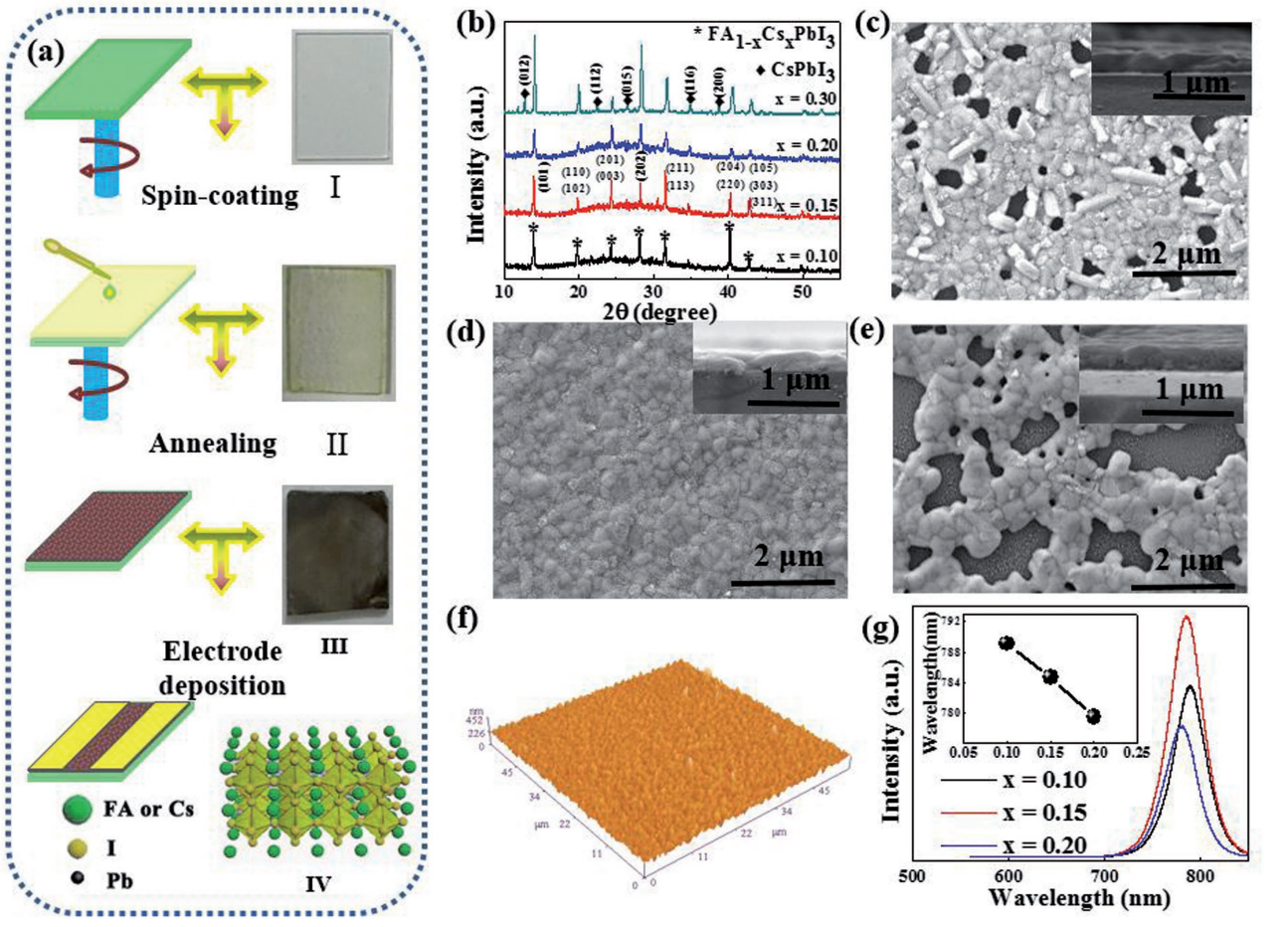

Figure 1. a) Schematic illustration of stepwise process for fabrication of the $FA_{1-x}Cs_xPbI_3$ perovskite film photodetector. b) X-ray diffraction (XRD) patterns of four $FA_{1-x}Cs_xPbI_3$ films with different doping levels. c–e) FESEM images of $FA_{1-x}Cs_xPbI_3$ perovskite films with different components ($x = 0.10$, 0.15, and 0.20, respectively), the insets of (c)–(e) show the corresponding cross-section SEM image of the perovskite film. f) Tapping-mode AFM height image of the $FA_{0.85}Cs_{0.15}PbI_3$ film. g) Steady-state photoluminescence spectra of the $FA_{1-x}Cs_xPbI_3$ film, the inset shows the peak location as a function of cesium level.

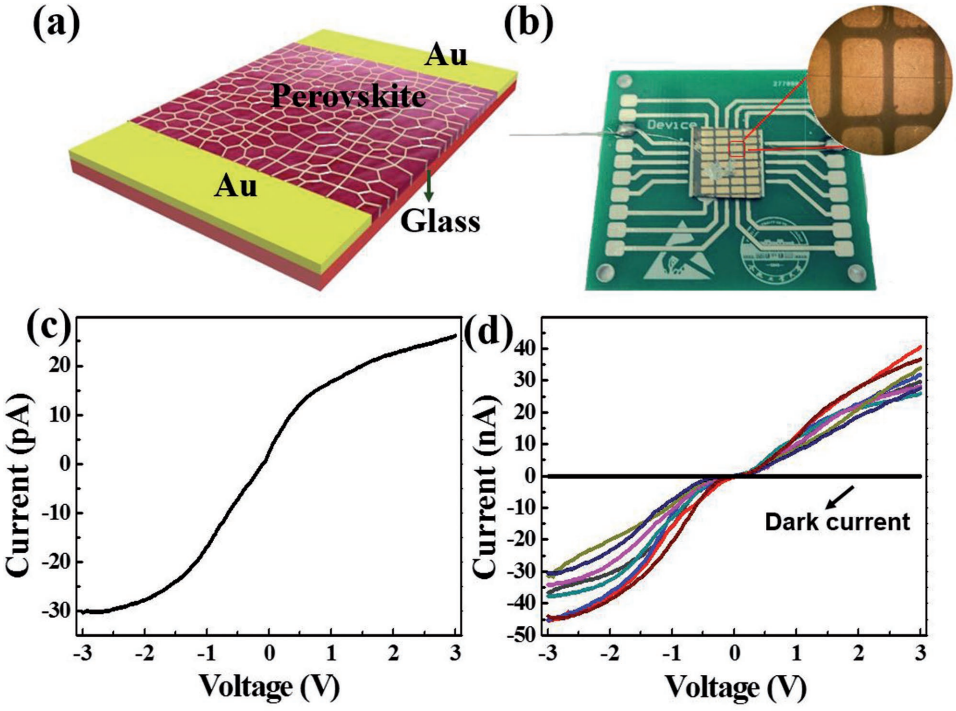

Figure 2. a) Schematic illustration of the $FA_{0.85}Cs_{0.15}PbI_3$ photodetector. b) A digital camera picture of the perovskite device on PCB. c) *I–V* curve of the perovskite film device in dark condition. d) *I–V* curves of representative eight devices under white light illumination.

Considering the relatively high quality of the $FA_{0.85}Cs_{0.15}PbI_3$, only thin film with this chemical composition was selected for photodetector fabrication. **Figure 2**a shows a schematic illustration of the perovskite film device composed of $FA_{0.85}Cs_{0.15}PbI_3$ thin film and two parallel gold electrodes (thickness: 50 nm). For convenience, the as-fabricated device was then fixed on a printed circuit board (PCB, Figure 2b). The *I–V* curves in dark were measured in air at room temperature (Figure 2c). It can be found that the current exhibits a linear characteristic, suggesting the formation of a good contact between $FA_{0.85}Cs_{0.15}PbI_3$ and Au electrodes with negligible contact barrier. Remarkably, once the $FA_{0.85}Cs_{0.15}PbI_3$ film device was shined by white light illumination, the current will increase dramatically. It should be pointed out that unlike other traditional inorganic semiconductor material-based devices,[22] the *I–V* curve of the present perovskite film photodetector under light illumination is nonlinear, particularly at small bias voltage. As a matter of fact, this behavior has been also confirmed by other representative eight devices, as shown in Figure 2d. This photoelectric characteristic, often observed in other perovskite devices composed of both $CH_3NH_3PbI_3$[23] and $CH_3NH_3PbCl_3$,[24] may be related to the surface trap states in view of the solution-based synthetic approach used in this study.

The above photosensitivity to white light is repeatable even after 90 cycles operation (Figure S1, Supporting Information), suggesting the excellent device reproducibility. Further *I–V* curves in **Figure 3**a reveals that this photoresponse is actually dependent on the incident light intensity, which is reasonable in that stronger illumination will generate more photon-excited electron–hole pairs, and therefore leads to higher photocurrent in the circuit. It was also observed that the photocurrent was highly related to bias voltage. Figure 3b plots the photocurrent at different bias voltages, from which the photocurrent was found to increase gradually with the increase of bias voltage. Such a bias voltage dependent photocurrent is contrary to the relationship between on/off ratio and bias voltage. As shown in Figure 3c, the on–off ratio is 6.3×10^3 at bias voltage of 0.5 V. When the bias voltage increases from 0.5 to 3 V, the on–off ratio will keep decreasing, and reaches a minimum value of 2.1×10^3 at 3.0 V. To further quantitatively assess the device performance of the $FA_{0.85}Cs_{0.15}PbI_3$ film, both responsivity (R) and specific detectivity (D^*) were calculated using the following equations[25,26]

$$R = \frac{I_\lambda - I_d}{P_\lambda A} \tag{1}$$

$$D^* = \frac{R_\lambda A^{1/2}}{(2eI_d)^{1/2}} \tag{2}$$

where I_λ is the photocurrent, I_d is the darkcurrent, P_λ is the incident intensity, A is the areas of the device, and e is the elementary charge, respectively. By using the above values and the two equations, both responsivity and specific detectivity were computed. Figure 3d plots the responsivity and specific detectivity at different bias voltages. Both device parameters are negatively correlated to light intensity. That is, the weaker the light intensity, the higher the R and D^* will be. In order to gain a competitive R and D^*, a very weak white light with intensity of 0.6 μW cm^{-2} was chosen to illuminate the device. Based on the values in Figure 3e, the R and D^* were estimated

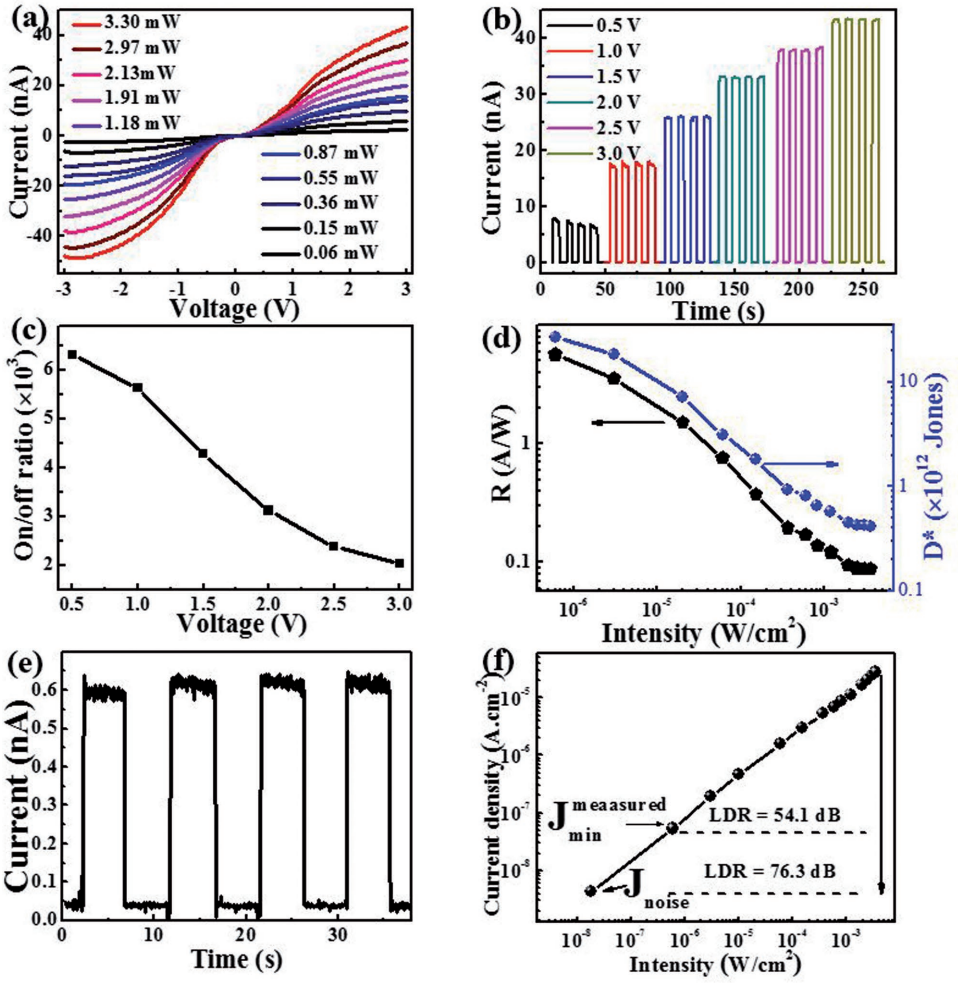

Figure 3. a) *I–V* characteristics of perovskite device under illumination of white light with different power intensities. b) Photoresponse of the devices under different bias voltages. c) The on/off ratio as a function of different voltage. d) Both responsivity and specific detectivity under white light illumination with different intensities. e) The photoresponse under light illumination with an intensity of 0.6 μW cm^{-2}. f) Photocurrent as a function of the incident intensity at a bias of 0.5 V.

to be 5.7 A W^{-1} and 2.7×10^{13} cm Hz$^{1/2}$ W^{-1} (the detailed calculation process is provided in the Supporting Information). Besides, the linear dynamic range (LDR) defined as the range in which the photocurrent has a linear response as the incident light intensity changes was also calculated by the following relation[27]

$$\mathrm{LDR} = 20\log(I_\mathrm{P}/I_\mathrm{d}) \tag{3}$$

where I_p and I_d are the photocurrent and darkcurrent, respectively, measured at light intensity of 0.06 and 3.3 mW cm^{-2}. The highest LDR are estimated to be 76.3 dB (Figure 3f). This value is higher than that of other types of photodetectors composed of InGaAs (66 dB)[28] and most 2D transition metal dichalcogenide (40–80 dB).[29]

Further photoresponse characteristics find that the photosensitivity of our $FA_{0.85}Cs_{0.15}PbI_3$ photodetector relies on the illumination wavelength. **Figure 4**a shows the *I–V* curves over a range of 400–800 nm under a fixed irradiation power of 120 μW cm^{-2}. One can learn that the photocurrent increases with the decrease of the wavelengths and reaches a maximum value at 400 nm. The photocurrent to each monochromatic light depends on the light intensity (Figure S2, Supporting Information), and the corresponding relationship can be fitted by a simple power law (Figure S3, Supporting Information). It is also interesting to observe that this perovskite photodetector exhibits good detection ability to the UV light (Figure 4b), and the photocurrent under UV light illumination is dependent on the incident UV intensity (Figure 4c) as well. By employing Equations (1) and (2), both responsivity and specific detectivity at different intensities are calculated and summarized in Figure 4d. Specifically, the highest *R* and *D** are estimated to be 0.1 A W^{-1} and 1.42×10^{12} cm Hz$^{1/2}$ W^{-1}, respectively, under illumination power of 12 μW cm^{-2}. By studying the photocurrent at a fixed light intensity with different wavelengths, the spectral photoresponse in the range from 240 to 800 nm was obtained. As plotted in Figure 4e, the perovskite device shows obvious photosensitivity to illumination with wavelength in the range from 240 to 750 nm, but the sensitivity will be rather low when the wavelength is longer than 750 nm,

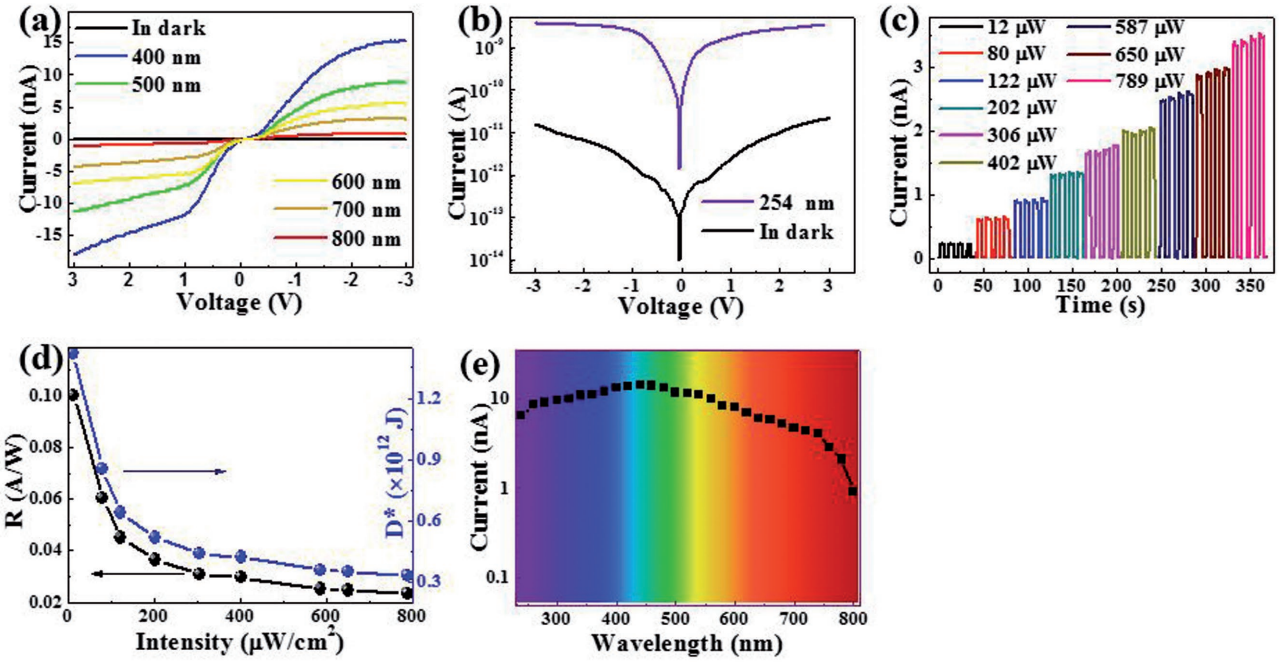

Figure 4. a) *I–V* characteristics of photodetector to light illumination with different wavelengths. b) The *I–V* characteristics curve with and without 254 nm illumination. c) The photoresponse to 254 nm with different light intensities. d) Both responsivity and specific detectivity of the perovskite heterojunction under 254 nm light illumination with different intensities. e) Spectral response of the device in the range from 240 to 800 nm.

which is consistent with the optical absorption curve reported previously.[21]

The response speed was then studied by using a home-made setup in which the perovskite photodetector was connected with the resistor (*R*) in series (**Figure 5**a). The pulsed incident light was generated by a laser diode driven by a high-frequency signal generator, which can provide pulsed light with a frequency as high as 10 MHz. Figure 5b–d illustrates the

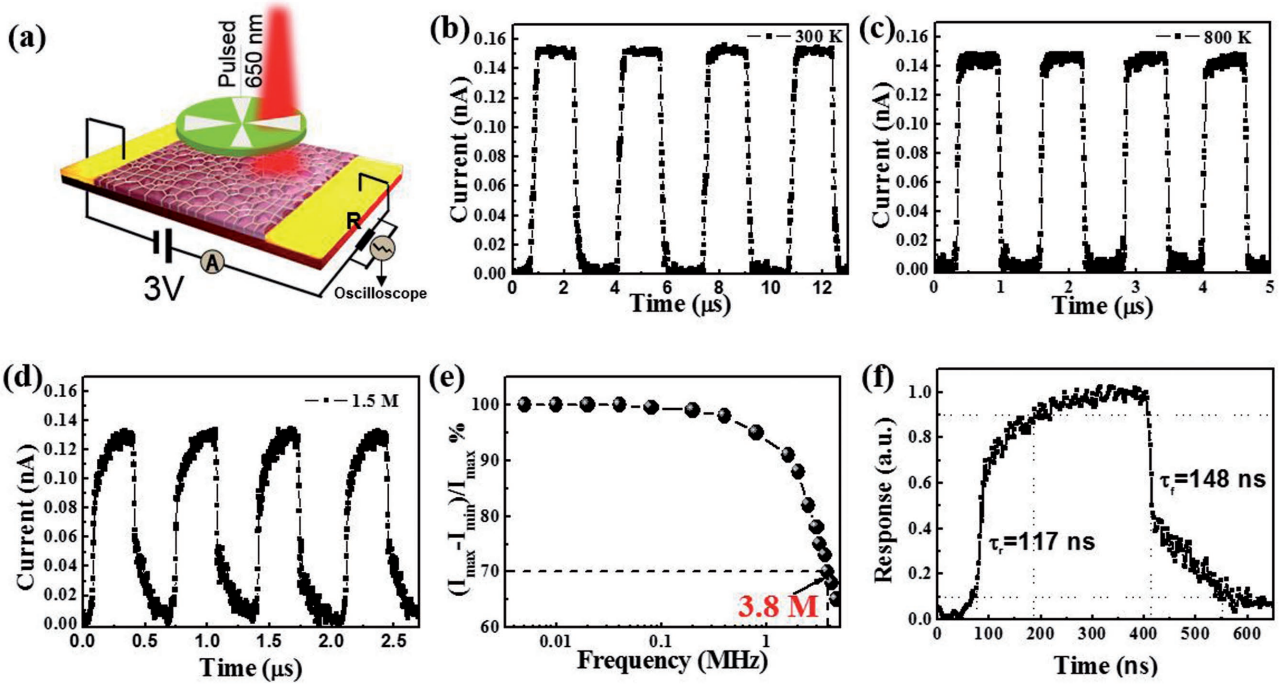

Figure 5. a) Schematic illustration of testing equivalent circuit at 3 V, the wavelength of incident light was 650 nm. Photocurrent of the perovskite photodetector under 650 nm light illumination with frequency of 300 KHz b), 800 KHz c), and 1.5 MHz, the bias voltage is 3 V. e) The relationship of $(I_{max} - I_{min})/I_{max}$ versus switching frequency. f) Single normalized cycle of the photodetector for estimating both rise time and fall time.

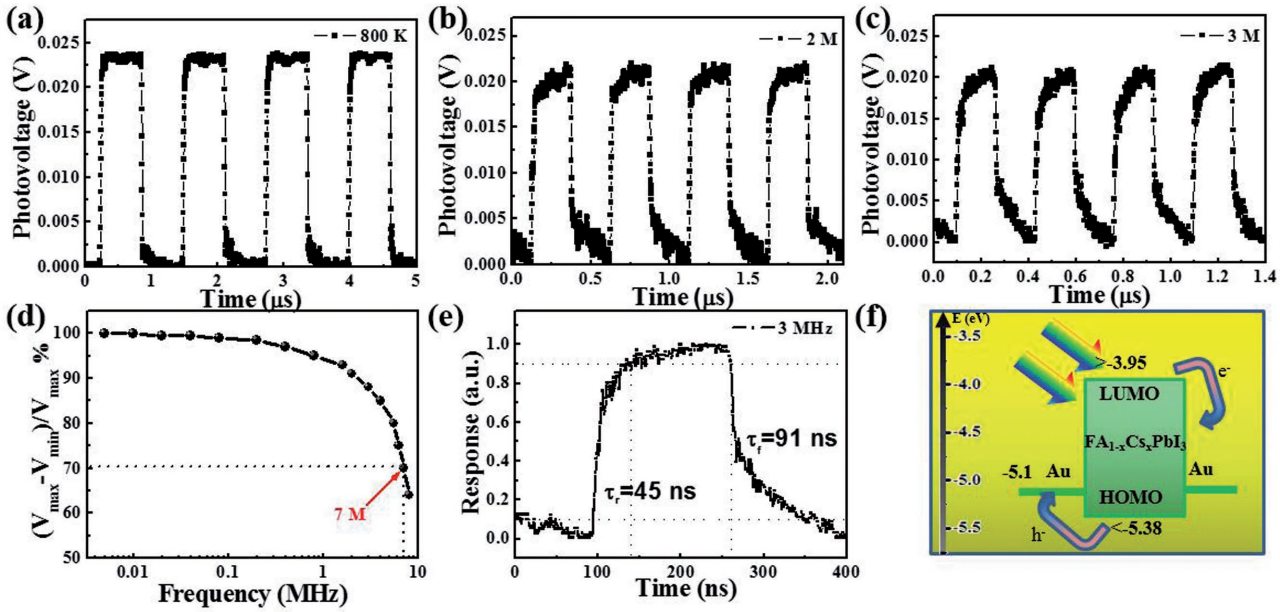

Figure 6. Photoresponse of the perovskite photodetector at a bias voltage of 0 V, with frequency of 800 KHz a), 1.6 MHz b), and 3 MHz c). d) The relationship of $(V_{max}-V_{min})/V_{max}$ versus switching frequency. e) Single normalized cycle of the photodetector for estimating both rise time and fall time. f) Energy band diagram of the perovskite photodetector under light illumination.

photocurrent recorded at 3 V under 650 nm with different frequencies. Obviously, for 300 KHz, 800 KHz, and 1.5 MHz, our perovskite device coherently demonstrates excellent switching characteristics when the incident 650 nm light was turned on and off repeatedly. The 3 dB bandwidth of the device was estimated to be 3.8 MHz (Figure 5e), suggesting the great potential of the present perovskite photodetector for detecting ultrafast-switching optical signal. A single normalized cycle at 1.5 M Hz was displayed in Figure 5f, from which the rise time and fall time are estimated to be 117 and 148 ns, respectively (The rise time (τ_r) is from 10% to 90% and the fall time (τ_f) is from 90% to 10% of its peak value).[30]

To our surprise, the response speed of the perovskite photodetector can be further accelerated once the bias voltage was revoked (For optoelectronic study at 0 V, the testing equivalent circuit was slightly modified, refer to Figure S4, Supporting Information). **Figure 6**a–c shows the reversible switching curves between low and high conductance states at frequency of 0.8, 2, and 3 MHz. From the relative balance result in Figure 6d, it can be concluded that the perovskite device shows a better 3dB bandwidth than that at 3 V. From the single normalized cycle shown in Figure 6e, the rise time and fall time were determined to be 45 ns and 91 ns, respectively, which are much better than the result at 3 V. Such ultrafast response speed is not only related to the unique optoelectronic property of the Cs-doped $FAPbI_3$ but also due to the Schottky junction at the Au/perovskite interface under light illumination, as indicated by Figure 2d. Figure 6f aligns the energy levels of the Au/$FA_{0.85}Cs_{0.15}PbI_3$/Au interfaces, the highest occupied molecular orbital and lowest unoccupied molecular orbital values were obtained from literature review.[20] Like conventional Schottky junction-based photovoltaic photodetector, the current metal–semiconductor interface is beneficial to response speed in that it is capable of swiftly separating photogenerated electron–hole pairs under light illumination.

On the other hand, the above ultrafast response speed is related to the ultrashort lifetime. The transient PL spectrum of the $FA_{0.85}Cs_{0.15}PbI_3$ device is studied in **Figure 7**a. By fitting the transient PL curve using a biexponential function $[I(t) = A_1e^{-\frac{t}{\tau_1}} + A_2e^{-\frac{t}{\tau_2}}$, where τ_1 (τ_2) represents the fast (slow) decay time; A_1 (A_2) represents the amplitude of the fast-decay (slow-decay) component at $t = 0$], a fast ($t_1 \approx 4.97$ ns) and slow ($t_2 \approx 20.1$ ns) dynamics for the perovskite film were obtained. According to previous study, these two values were associated with the surface (fast) and bulk (slow) recombination, respectively.[31] This ultrashort lifetime derived from a perovskite materials with a relatively low trap density seems to deviate some the materials in Figure 7b, but it is comparable to that of $CH_3NH_3PbI_3$ nanowires.[32] Considering the fact that for a given semiconductor material, there are also other factors such as processing condition, doping level and surface states that can influence the lifetime, we therefore believe that our measurement as well as the experimental results are trustworthy. Such an ultrafast lifetime is undoubtedly instrumental to the fast response speed. The third contributory factor for the fast response speed is the high quality of the perovskite material. Figure 7c shows the carrier mobility and trap density of four representative device's using the Hall effect method, through which the average electron mobility (μ_n) and trap density (n_{trap}) were estimated to be 133.5 $cm^2\ s^{-1}\ V^{-1}$ and $1.75 \times 10^{13}\ cm^{-3}$, respectively (Figure S5, Supporting Information). Figure 7d,e compare the electron mobility and defect concentrations of these materials with recently reported results. Obviously, the $FA_{0.85}Cs_{0.15}PbI_3$ device is comparable to other perovskite thin film, but the defect concentration is relatively lower than

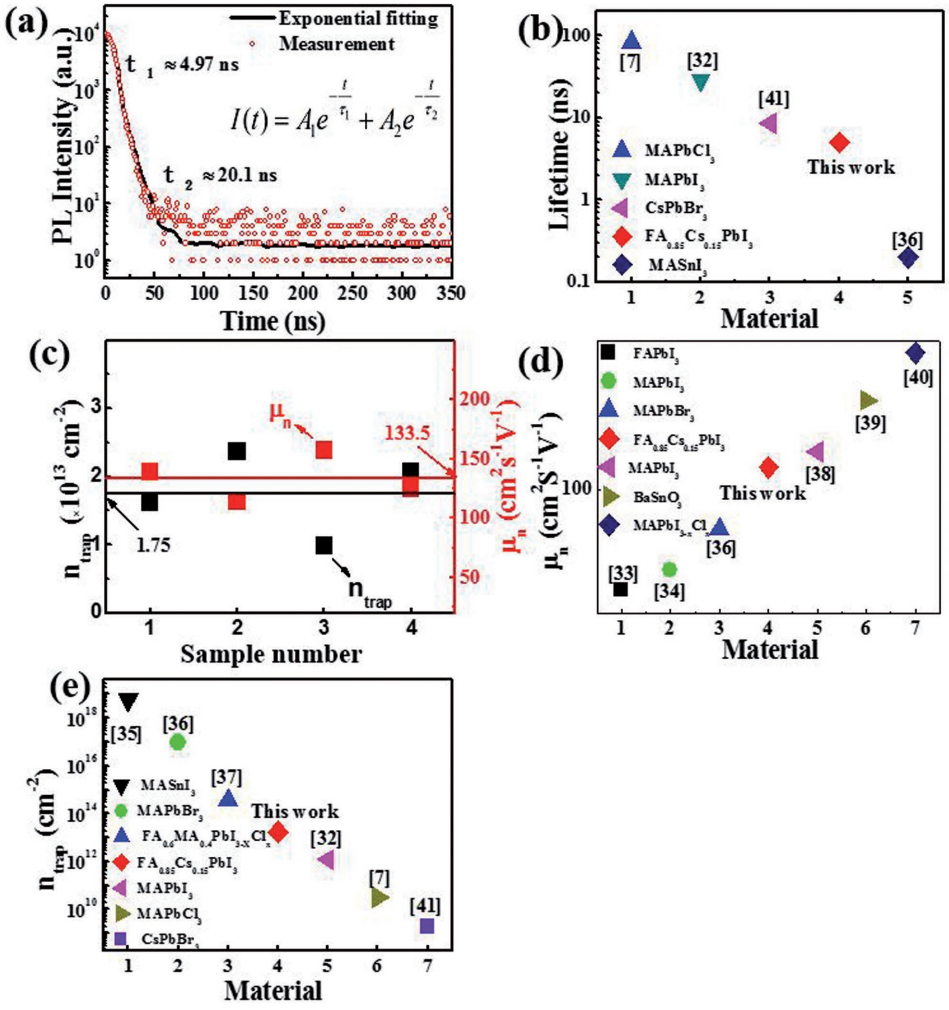

Figure 7. a) Time-resolved photoluminescence spectral with biexponential fits. b) Comparison of lifetime of the $FA_{0.85}Cs_{0.15}PbI_3$ film and other perovskite films. c) The Hall carrier mobility and trap density of four devices. d) Comparison of carrier mobility of the $FA_{0.85}Cs_{0.15}PbI_3$ film and other perovskite film. e) Comparison of trap density concentration of the $FA_{0.85}Cs_{0.15}PbI_3$ and other perovskite films.

other perovskite materials with similar carrier lifetime.[33–41] Such a relatively low defect concentration leads to a long diffusion length, which can be calculated by the following two equations[38]

$$D = \frac{\mu K_B T}{q} \tag{4}$$

$$L = \sqrt{D.\tau} \tag{5}$$

where D is diffusion length coefficient, L is the diffusion length, K_B is the Boltzmann's constant, T is the temperature of the sample, q is the elementary charge, and τ is the carrier bulk recombination lifetime, respectively. The carrier diffusion length (L) is calculated to be 2.6 μm. Such a value is better than the $MAPbI_3$ (≈1 μm)[42] and $MAPbBr_3$ polycrystalline film (≈0.33 μm),[36] and therefore is beneficial for the excellent optoelectronic property mentioned above.[43]

Table 1 compares some device parameters including the bias voltage, response time, responsivity and specific detectivity, and other perovskite-based devices. The response speed is 45/91 ns (rise time/fall time), which represent the best results reported. What is more, the R and D^* are comparable to or slightly smaller than the devices based on $MAPbI_3$ nanowires and $MAPbI_{3-x}Cl_x$ film[32,49,50] but are much better than the devices composed of $CsPbBr_3$ and $CsPbI_3$ nanocrystals,[47,48] $MAPbBr_{3-x}I_x$ film,[50] and $MAPbI_3$ and $MAPbCl_3$ single crystal.[7,23] Without doubt, the relatively good device performance as well as the broadband spectral response renders the present photodetector highly promising for future photosensing applications.

In addition to the obvious advantages mentioned above, the present $FA_{0.85}Cs_{0.15}PbI_3$ thin film photodetector displays a stable sensitivity to light illumination after 45 days storage in air, even though the phase has changed. **Figure 8**a shows the photocurrent evolution to both white light and 254 nm light illumination after storage for different durations (from one week to 45 days). One can see clearly that after 45 days storage, the photocurrent under 254 nm illumination decreased by nearly

Table 1. Comparison of device performance of our device and other perovskite materials-based photodetectors.

Materials	Bias [V]	τ_r/τ_f	R [A W^{-1}]	D^* [Jones]	Reference
$FA_{0.85}Cs_{0.15}PbI_3$ film	0	45/91 ns	5.7	2.7×10^{13}	This work
$MAPbCl_3$ single crystals	15	24/62 ms	0.047	1.2×10^{10}	[7]
$MAPbI_3$ single crystals	3	74/58 µs	2.55	–	[23]
$MAPbI_3$ nanowires	1	<0.1 ms	4.95	2.0×10^{13}	[32]
$MAPbI_3$ film	3	100/100 ms	3.49	–	[44]
$MAPbI_3$ network	10	0.3/0.4 ms	0.1	1.02×10^{12}	[45]
$MAPbCl_3$ single crystals	5	–/1 ms	18	10^{12}	[46]
$CsPbBr_3$ nanocrystals	3	1.8/1.0 ms	0.18	6.1×10^{10}	[47]
$CsPbI_3$ nanocrystals	1	24/29 ms	–	–	[48]
$MAPbI_{3-x}Cl_x$ film	0.1	180/160 ns	–	8.0×10^{13}	[49]
$MAPbBr_{3-x}I_x$ film	10	20/20 µs	0.055	–	[50]

ne order of magnitude. This completely differs from the photosensitivity to white light illumination, which only decreases by 25%, from 4.1×10^{-9} to 3×10^{-9} nA. Such a wavelength dependent photocurrent evolution is understandable given the fact that the structure of perovskite material has changed after long-term storage at ambient condition. Figure 8b compares the XRD patterns of $FA_{0.85}Cs_{0.15}PbI_3$ film before and after 45 days. It can be clearly seen that besides the $FA_{0.85}Cs_{0.15}PbI_3$ phase, new diffraction peaks attributable to $CsPbI_3$ and unknown phase begins to come into being. The newly formed materials have a different sensitivity to light illumination than the Cs-doped $FaPbI_3$: It is sensitive to the visible light illumination, but it is blind to deep UV light. As a result, the photodetector exhibits relatively good sensitivity to white light than the UV light.

3. Conclusion

In summary, a high-performance broadband perovskite photodetector has been successfully fabricated by a simple spin-coating synthesis process. Device performance analysis finds that the as-fabricated device exhibits high sensitivity to broadband illumination, with wavelength in the range from 240 to 750 nm. What is more, the perovskite photodetector is capable of detecting 3 MHz optical signal at zero bias voltage, with a high response speed (rise/fall time of 45/91 ns). In addition, the R and D^* of the device are estimated to be 5.7 A W^{-1} and 2.7×10^{13} cm Hz$^{1/2}$ W^{-1}, respectively. Finally, this device is observed to exhibit good photosensitivity to white light illumination after storage at ambient condition for 45 days. The broadband sensitivity, high specific detectivity, and fast response speed corroborate that the $FA_{1-x}Cs_xPbI_3$ perovskite-based photodetector is greatly promising for future optoelectronic devices application.

4. Experimental Section

Synthesis and Characterization of $FA_{1-x}Cs_xPbI_3$ Perovskite Film: The $FA_{1-x}Cs_xPbI_3$ thin film was synthesized through a modified one-step spin-coating method.[21] First, 461 mg PbI_2 (Aldrich, 99%), different amount of FAI (Aldrich, 99.5%), and CsI (Aldrich, 99.9%) were added sequentially into a mixed solution of 200 µL dimethyl sulfoxide (>99.9%) and 800 µL *N*,*N*-dimethylformamide (99.8%). To form different alloy compositions (x = 0.10, 0.15, and 0.20), the FAI used was 137, 145, and 154 mg while the CsI 26, 39, and 52 mg, respectively. The mixture was stirred at 70 °C for 1 h in a flask. Then 30 µL of the as-prepared perovskite precursor was spin coated onto the glass substrate at a speed of 4000 rpm. After 10 s, 500 µL diethyl ether solution (99.0%) was dropped onto the perovskite film. After spin coating for another 50 s, the substrate was first heated up to 50 °C for 3 min and then 140 °C for 15 min. Finally, the $FA_{1-x}Cs_xPbI_3$ perovskite film in black-brownish color was obtained. The XRD patterns of the perovskite films were recorded using an X-ray diffractormeter (Rigaku D/max-rB). The AFM image of the film was obtained from an atomic force microscopy (Benyuan Nanotech Com., CSPM-4000). The morphology of the thin film was examined by a field-emission SEM (FESEM, SIRION 200 FEG). The photoluminescence was explored by a confocal laser Raman spectrometer (Horiba Jobin Yvon, Labram HR evolution).

Device Fabrication and Analysis: To fabricate the perovskite film-based photodetectors, parallel Au metal electrodes with thickness of around 50 nm were deposited via electron-beam evaporator, with the assistance of a shadow mask. The channel length (L) and width (W) are 1 mm and 18 µm, respectively. The electrical measurements were performed using a semiconductor I–V characterization system (Keithley Company, 4200-SCS). For optoelectronic property study, several kinds of laser diodes (Tanon Company, UV-100) with different wavelengths (254, 450, 650, and 808 nm) were used to illuminate the device. For response speed study, the device was shined by a laser diode driven by a high-frequency signal generator, and the pulsed voltage was recorded by an

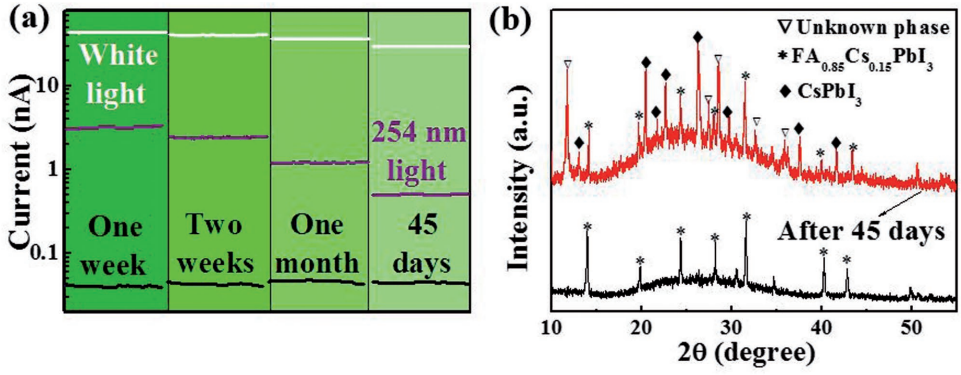

Figure 8. a) Photoresponse of $FA_{0.85}Cs_{0.15}PbI_3$ photodetector to both white light and 254 nm light illumination, after storage in air for varied times. b) Comparison of the XRD pattern of $FA_{0.85}Cs_{0.15}PbI_3$ film before and after 45 d storage.

oscilloscope (Tektronix, TDS2012B). Note that the power intensity of the incident light was calibrated by a powermeter (Thorlabs GmbH., PM 100D) prior to use.

Supporting Information

Supporting Information is available from the Wiley Online Library or from the author.

Acknowledgements

This work was supported by the National Natural Science Foundation of China (NSFC, Nos. 21501038, 61575059, and 61675062), the Fundamental Research Funds for the Central Universities (2013HGCH0012 and 2014HGCH0005), and the China Postdoctoral Science Foundation (103471013).

Conflict of Interest

The authors declare no conflict of interest.

Keywords

formamidinium, optoelectronic devices, perovskite materials, response speed, specific detectivity

Received: July 5, 2017
Revised: August 4, 2017
Published online:

[1] X. Gong, M. H. Tong, Y. J. Xia, W. Z. Cai, J. S. Moon, Y. Cao, G. Yu, C. L. Shieh, B. Nilsson, A. J. Heeger, *Science* **2009**, *325*, 1665.
[2] Q. Liu, L. Jiang, X. M. Zou, X. H. Xiao, S. S. Guo, C. Z. Jiang, X. Liu, Z. Y. Fan, W. D. Hu, X. S. Chen, W. Lu, W. P. Hu, L. Liao, *Adv. Mater.* **2014**, *26*, 2919.
[3] S. Miao, W. D. Hu, N. Guo, Z. Y. Lu, X. M. Zou, L. Liao, S. X. Shi, P. P. Chen, Z. Y. Fan, J. C. Ho, T. X. Li, X. S. Chen, W. Lu, *ACS Nano* **2014**, *8*, 3658.
[4] T. Gao, Q. Zhang, J. N. Chen, X. Xiong, T. Y. Zhai, *Adv. Opt. Mater.* **2017**, *5*, 1700206.
[5] W. Deng, L. M. Huang, X. Z. Xu, X. J. Zhang, X. C. Jin, S. T. Lee, J. S. Jie, *Nano Lett.* **2017**, *17*, 2482.
[6] L. Gao, C. Chen, K. Zeng, C. Ge, D. Yang, H. S. Song, J. Tang, *Light: Sci. Appl.* **2016**, *5*, e16126.
[7] G. Maculan, A. D. Sheikh, A. L. Abdelhady, M. I. Saidaminov, M. A. Haque, B. Murali, E. Alarousu, O. F. Mohammed, T. Wu, O. M. Bakr, *J. Phys. Chem. Lett.* **2015**, *6*, 3781.
[8] D. B. Li, L. Hu, Y. Xie, G. D. Niu, T. F. Liu, Y. H. Zhou, L. Gao, B. Yang, J. Tang, *ACS Photonics* **2016**, *3*, 2122.
[9] M. Y. Leng, Z. W. Chen, Y. Yang, Z. Li, K. Zeng, K. H. Li, G. D. Niu, Y. S. He, Q. C. Zhou, J. Tang, *Angew. Chem. Int. Ed.* **2016**, *55*, 15012.
[10] J. Seo, J. H. Noh, S. I. Seok, *Acc. Chem. Res.* **2016**, *49*, 562.
[11] X. S. Tang, Z. P. Hu, W. Yuan, W. Hu, H. B. Shao, D. J. Han, J. F. Zheng, J. Y. Hao, Z. G. Zang, J. Du, Y. X. Leng, L. Fang, M. Zhou, *Adv. Opt. Mater.* **2017**, *5*, 1600788.
[12] X. L. Zhang, W. G. Wang, B. Xu, S. Liu, H. T. Dai, D. Bian, S. M. Chen, K. Wang, X. W. Sun, *Nano Energy* **2017**, *37*, 40.
[13] Y. L. Guo, C. Liu, H. Tanaka, E. Nakamura, *J. Phys. Chem. Lett.* **2015**, *6*, 535.
[14] Y. Lee, J. Kwon, E. Hwang, C. H. Ra, W. J. Yoo, J. H. Ahn, J. H. Park, J. H. Cho, *Adv. Mater.* **2015**, *27*, 41.
[15] W. Deng, X. J. Zhang, L. M. Huang, X. Z. Xu, L. Wang, J. C. Wang, Q. X. Shang, S. T. Lee, J. S. Jie, *Adv. Mater.* **2016**, *28*, 2201.
[16] J. X. Ding, S. J. Du, Z. Y. Zuo, Y. Zhao, H. Z. Cui, X. Y. Zhan, *J. Phys. Chem. C* **2017**, *121*, 4917.
[17] H. J. Fang, Q. Li, J. Ding, N. Li, H. Tian, L. J. Zhang, T. L. Ren, J. Y. Dai, L. D. Wang, Q. F. Yan, *J. Mater. Chem. C* **2016**, *4*, 630.
[18] X. L. Zhang, H. Liu, W. G. Wang, J. B. Zhang, B. Xu, K. L. Karen, Y. J. Zheng, S. Liu, S. M. Chen, K. Wang, X. W. Sun, *Adv. Mater.* **2017**, *29*, 1606405.
[19] S. P. Pang, H. Hu, J. L. Zhang, S. L. Lv, Y. M. Yu, F. Wei, T. S. Qin, H. X. Xu, Z. H. Liu, G. L. Cui, *Chem. Mater.* **2014**, *26*, 1485.
[20] X. Xia, W. Y. Wu, H. C. Li, B. Zheng, Y. Xue, J. B. Xu, D. W. Zhang, C. X. Gao, X. Z. Liu, *RSC Adv.* **2016**, *6*, 14792.
[21] J. W. Lee, D. H. Kim, H. S. Kim, S. W. Seo, S. M. Cho, N. G. Park, *Adv. Energy Mater.* **2015**, *5*, 1501310.
[22] J. S. Jie, W. J. Zhang, Y. Jiang, X. M. Meng, Y. Q. Li, S. T. Lee, *Nano Lett.* **2006**, *6*, 1887.
[23] Z. P. Lian, Q. F. Yan, Q. R. Lv, Y. Wang, L. L. Liu, L. J. Zhang, S. L. Pan, Q. Li, L. D. Wang, J. L. Sun, *Sci. Rep.* **2015**, *5*, 16563.
[24] W. Z. Wang, H. T. Xu, J. Cai, J. B. Zhu, C. W. Ni, F. Hong, Z. B. Fang, F. Z. Xu, S. W. Cui, R. Xu, L. J. Wang, F. Xu, J. Huang, *Opt. Express* **2016**, *24*, 8411.
[25] W. Y. Kong, G. A. Wu, K. Y. Wang, T. F. Zhang, Y. F. Zou, D. D. Wang, L. B. Luo, *Adv. Mater.* **2016**, *28*, 10725.
[26] B. Nie, J. G. Hu, L. B. Luo, C. Xie, L. H. Zeng, P. Lv, F. Z. Li, J. S. Jie, M. Feng, C. Y. Wu, Y. Q. Yu, S. H. Yu, *Small* **2013**, *9*, 2872.
[27] G. Q. Tong, X. S. Geng, Y. Q. Yu, L. W. Yu, J. Xu, Y. Jiang, Y. Sheng, Y. Shi, K. J. Chen, *RSC Adv.* **2017**, *7*, 18224.
[28] L. T. Dou, Y. M. Yang, J. B. You, Z. R. Hong, W. H. Chang, G. Li, Y. Yang, *Nat Commun.* **2014**, *5*, 5404.
[29] X. S. Geng, Y. Q. Yu, X. L. Zhou, C. D. Wang, K. W. Xu, Y. Zhang, C. Y. Wu, L. Wang, Y. Jiang, Q. Yang, *Nano Res.* **2016**, *9*, 2641.
[30] L. H. Zeng, M. Z. Wang, H. Hu, B. Nie, Y. Q. Yu, C. Y. Wu, L. Wang, J. G. Hu, C. Xie, F. X. Liang, L. B. Luo, *ACS Appl. Mater. Interfaces* **2013**, *5*, 9362.
[31] H. S. Rao, W. G. Li, B. X. Chen, D. B. Kuang, C. Y. Su, *Adv. Mater.* **2017**, *29*, 1602639.
[32] L. Gao, K. Zeng, J. S. Guo, C. Ge, J. Du, Y. Zhao, C. Chen, H. Deng, Y. S. He, H. S. Song, G. D. Niu, J. Tang, *Nano Lett.* **2016**, *16*, 7446.
[33] W. Rehman, R. L. Milot, G. E. Eperon, C. Wehrenfennig, J. L. Boland, H. J. Snaith, M. B. Johnston, L. M. Herz, *Adv. Mater.* **2015**, *27*, 7938.
[34] R. L. Milot, G. E. Eperon, H. J. Snaith, M. B. Johnston, L. M. Herz, *Adv. Funct. Mater.* **2015**, *25*, 6218.
[35] N. K. Noel, S. D. Stranks, A. Abate, C. Wehrenfennig, S. Guarnera, A. A. Haghighirad, A. Sadhanala, G. E. Eperon, S. K. Pathak, M. B. Johnston, A. Petrozza, L. M. Herz, H. J. Snaith, *Energy Environ. Sci.* **2014**, *7*, 3061.
[36] M. I. Saidaminov, V. Adinolfi, R. Comin, A. L. Abdelhady, W. Peng, I. Dursun, M. J. Yuan, S. Hoogland, E. H. Sargent, O. M. Bakr, *Nat. Commun.* **2015**, *6*, 8724.
[37] D. H. Kim, J. Park, Z. Li, M. J. Yang, J. S. Park, I. J. Park, J. Y. Kim, J. J. Berry, G. Rumbles, K. Zhu, *Adv. Mater.* **2017**, *29*, 1606831.
[38] Q. F. Dong, Y. J. Fang, Y. C. Shao, P. Mulligan, J. Qiu, L. Cao, J. S. Huang, *Science* **2015**, *347*, 967.

[39] H. J. Kim, U. Kim, H. M. Kim, T. H. Kim, H. S. Mun, B.-G. Jeon, K. T. Hong, W.-J. Lee, C. Ju, K. H. Kim, K. Char, *Appl. Phys. Express* **2012**, *5*, 061102.
[40] F. Li, H. Wang, D. Kufer, L. L. Liang, W. L. Yu, E. Alarousu, C. Ma, Y. Y. Li, Z. X. Liu, C. X. Liu, N. N. Wei, F. Wang, L. Chen, O. F. Mohammed, A. Fratalocchi, X. G. Liu, G. Konstantatos, T. Wu, *Adv. Mater.* **2017**, *29*, 1602432.
[41] J. Z. Song, Q. Z. Cui, J. H. Li, J. Y. Xu, Y. Wang, L. M. Xu, J. Xue, Y. H. Dong, T. Tian, H. D. Sun, H. B. Zeng, *Adv. Opt. Mater.* **2017**, *5*, 1700157.
[42] S. Yakunin, M. Sytnyk, D. Kriegner, S. Shrestha, M. Richter, G. J. Matt, H. Azimi, C. J. Brabec, J. Stangl, M. V. Kovalenko, W. Heiss, *Nat. Photonics* **2015**, *9*, 444.
[43] H. L. Wang, R. Haroldson, B. Balachandran, A. Zakhidov, S. Sohal, J. Y. Chan, A. Zakhidov, W. Hu, *ACS Nano* **2016**, *10*, 10921.
[44] X. Hu, X. D. Zhang, L. Liang, J. Bao, S. Li, W. L. Yang, Y. Xie, *Adv. Funct. Mater.* **2014**, *24*, 7373.
[45] H. Deng, X. Yang, D. Dong, B. Li, D. Yang, S. Yuan, K. Qiao, Y. B. Cheng, J. Tang, H. Song, *Nano Lett.* **2015**, *15*, 7963.
[46] V. Adinolfi, O. Ouellette, M. I. Saidaminov, G. Walters, A. L. Abdelhady, O. M. Bakr, E. H. Sargent, *Adv. Mater.* **2016**, *28*, 7264.
[47] X. Li, D. Yu, F. Cao, Y. Gu, Y. Wei, Y. Wu, J. Song, H. Zeng, *Adv. Funct. Mater.* **2016**, *26*, 5903.
[48] P. Ramasamy, D. H. Lim, B. Kim, S. H. Lee, M. S. Lee, J. S. Lee, *Chem. Commun.* **2016**, *52*, 2067.
[49] L. T. Dou, Y. M. Yang, J. B. You, Z. R. Hong, W. H. Chang, G. Li, Y. Yang, *Nat. Commun.* **2014**, *5*, 5404.
[50] F. Wang, J. J. Mei, Y. P. Wang, L. G. Zhang, H. F. Zhao, D. X. Zhao, *ACS Appl. Mater. Interfaces* **2016**, *8*, 2840.